Structural Determinants of Phosphoinositide 3-Kinase Inhibition by Wortmannin, LY294002, Quercetin, Myricetin, and Staurosporine

Edward H. Walker,* Michael E. Pacold,* Olga Perisic,*
Len Stephens,† Philip T. Hawkins,†
Matthias P. Wymann,‡ and Roger L. Williams*§
*MRC Laboratory of Molecular Biology
MRC Centre
Hills Road, Cambridge CB2 2QH
United Kingdom
†Department of Signalling
Inositide Laboratory
Babraham Institute
Cambridge CB2 4AT
United Kingdom
‡Institute of Biochemistry
University of Fribourg
CH-1700 Fribourg
Switzerland

Summary

The specific phosphoinositide 3-kinase (PI3K) inhibitors wortmannin and LY294002 have been invaluable tools for elucidating the roles of these enzymes in signal transduction pathways. The X-ray crystallographic structures of PI3Kγ bound to these lipid kinase inhibitors and to the broad-spectrum protein kinase inhibitors quercetin, myricetin, and staurosporine reveal how these compounds fit into the ATP binding pocket. With a nanomolar IC_{50}, wortmannin most closely fits and fills the active site and induces a conformational change in the catalytic domain. Surprisingly, LY294002 and the lead compound on which it was designed, quercetin, as well as the closely related flavonoid myricetin bind PI3K in remarkably different orientations that are related to each other by 180° rotations. Staurosporine/PI3K interactions are reminiscent of low-affinity protein kinase/staurosporine complexes. These results provide a rich basis for development of isoform-specific PI3K inhibitors with therapeutic potential.

Introduction

Phosphoinositide 3-kinases phosphorylate phosphoinositides at the 3-hydroxyl. PI3Ks fall into three classes based on their primary structure and substrate specificity (reviewed in Domin and Waterfield, 1997; Toker and Cantley, 1997; Vanhaesebroeck and Waterfield, 1999). The class I PI3Ks can use phosphatidylinositol 4,5-bisphosphate (PIP_2) as a substrate to generate the second messenger PIP_3 and act as transducers downstream of tyrosine kinase receptors and G protein–coupled receptors. PI3Ks are involved in a large number of fundamental cellular processes, including apoptosis, proliferation, cell motility, and adhesion. The 3-phosphorylated phospholipids generated by PI3Ks act as membrane tethers

§To whom correspondence should be addressed (e-mail: rlw@mrc-lmb.cam.ac.uk).

for proteins such as protein kinase B (PKB) and phospholipid-dependent kinase 1 (PDK1). These are important components of the molecular mechanisms of diseases such as diabetes, cancer, and chronic inflammation. The class I isozymes are subdivided into classes IA and IB, with each subtype having a different regulatory subunit. The class IA enzymes (α, β, and δ) have a p85 regulatory subunit containing two SH2 domains, which are essential for their activation by tyrosine kinase receptors. The class IB PI3Kγ has a p101 subunit, which is required for maximal G$\beta\gamma$-stimulated formation of PIP_3 (Stephens et al., 1997; Krugmann et al., 1999; Maier et al., 1999).

The prominent roles that PI3Ks play in a variety of diseases have fueled intense efforts at developing isotype-specific inhibitors of PI3Ks. Wortmannin and its analogs were shown to inhibit phagocytocis-induced respiratory burst (Baggiolini et al., 1987). Subsequent work established that this is due to specific inhibition of PI3K activity. Recent reports of PI3Kγ knockout mice have shown that this isozyme plays a crucial role in inflammation (Hirsch et al., 2000; Li et al., 2000; Sasaki et al., 2000) and is required for macrophage motility and for G protein–coupled receptor activation of the respiratory burst. Because the knockout mice appeared otherwise normal, isotype-specific PI3Kγ inhibitors might be an effective means of controlling chronic inflammation. PI3Ks also have a role in cancer. Increased levels of PI3K products have been seen in colorectal tumors (Phillips et al., 1998) and in breast cancers (Gershtein et al., 1999). Dephosphorylation of PI3K products by the lipid-phosphatase activity of PTEN supresses tumor formation (Myers et al., 1998; Wu et al., 1998; Cantley and Neel, 1999). The PI3K inhibitors wortmannin and LY294002 have been crucial in deciphering the roles of PI3Ks in cellular processes. Both isotype-specific PI3K inhibitors and inhibitor-insensitive mutants of PI3K could greatly facilitate these studies.

Most protein kinase inhibitors that have been developed for pharmaceutical applications work by competing with ATP binding. Despite the overall similarity of the ATP binding sites among protein kinases, it has been possible to exploit differences in the modes of ATP interaction in order to develop protein kinase–specific inhibitors (Toledo et al., 1999). This has led to promising clinical applications (Garcia-Echeverria et al., 2000). In order to facilitate similar developments for the PI3Ks, we undertook the structure determination of PI3K. We recently determined the structure of porcine PI3Kγ both free and in a complex with ATP (Walker et al., 1999). The structure shows a multidomain organization, with the catalytic domain of PI3K having a similar fold to that of the protein kinases. The catalytic domain has two lobes: a smaller N-terminal lobe consisting of a five-stranded β sheet flanked by three α helices and a larger, primarily helical C-terminal lobe. The ATP cosubstrate binds between these lobes in a manner similar to ATP binding in protein kinases, with many of the enzyme/ATP contacts involving residues in the linker between the two lobes.
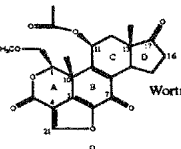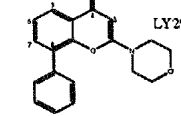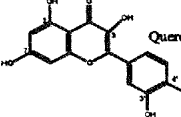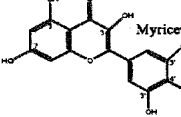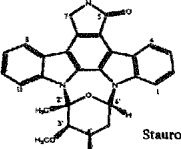
	Reported IC_{50}	K_d for PI3K γ
Wortmannin	4.2 nM (Class IA PI3K)	-
LY294002	1.4 μM (Bovine brain PI3K)	0.21 μM±0.04 μM
Quercetin	3.8 μM (Bovine brain PI3K)	0.28 μM±0.04 μM
Myricetin	1.8 μM (Class IA PI3K)	0.17 μM±0.04 μM
Staurosporine	9 μM* (Class IA PI3K)	0.29 μM±0.06 μM

Figure 1. Inhibitors of PI3K and Their Binding Characteristics to the Enzyme in Solution

Beside each compound is a representative IC_{50} for PI3K inhibition. The dissociation constants (K_d) for PI3Kγ as measured in the fluorescence assays are also shown along with the error in the least-squares fit.

The asterisk indicates that the reported IC_{50} is for 4′-N-benzoyl staurosporine.

We report here the X-ray crystallographic structures of porcine PI3Kγ in complexes with wortmannin, LY294002, quercetin, and myricetin as well as human PI3Kγ both free and in a complex with staurosporine (Figure 1). Wortmannin was originally isolated from *Penicillium wortmannii* (Brian et al., 1957) and was subsequently shown to be a specific inhibitor of PI3K with a low nanomolar IC_{50} (Arcaro and Wymann, 1993; Yano et al., 1993; Ui et al., 1995). LY294002 is a synthetic compound that was designed as a PI3K inhibitor based on the flavonoid quercetin (Vlahos et al., 1994). Although the reported IC_{50} of LY294002 is about 500-fold higher than that of wortmannin, LY294002 is widely used in cell biology as a specific PI3K inhibitor because it is much more stable in solution than wortmannin. For comparison with ATP analog inhibitor binding by protein kinases, we have determined the structures of PI3K with the broad-spectrum protein kinase inhibitors quercetin, myricetin, and staurosporine. Quercetin and myricetin are naturally occurring flavonoids that can inhibit a broad range of protein kinases (Srivastava, 1985). Quercetin and its analogs are also inhibitors of PI3K and have IC_{50}s of 1.8–20 μM (Matter et al., 1992; Agullo et al., 1997). The microbial alkaloid staurosporine is a highly
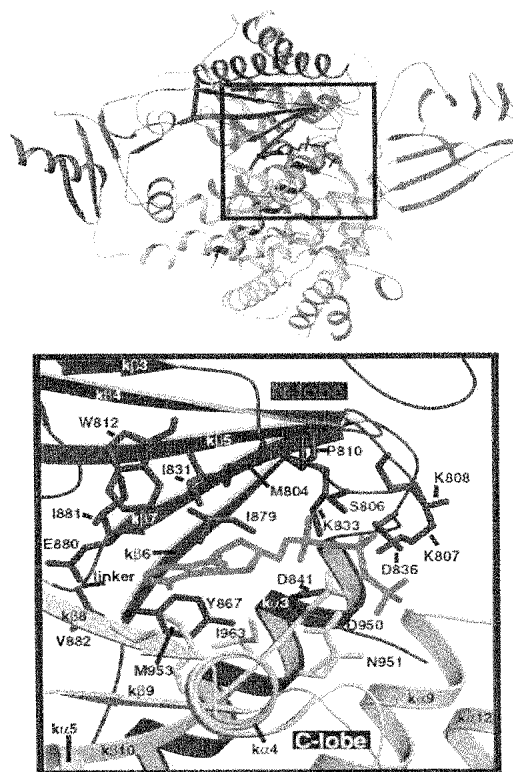

Figure 2. The ATP Binding Site of PI3Kγ

The upper panel illustrates the overall structure of the enzyme, consisting of a Ras-binding domain (magenta), a C2 domain (cyan), a helical domain (green), and a catalytic domain that has two lobes (N-terminal lobe colored red and C-terminal lobe colored yellow). The square highlights the ATP binding site that is shown in more detail in the lower panel. The ATP (green) bound to the enzyme and the side chains of all residues contacting ATP or any of the five inhibitors described here are shown in stick representation. The figure was prepared using Molscript (Kraulis, 1991) and Raster3D (Merritt and Bacon, 1997).

potent but nonspecific protein kinase inhibitor with a range of biological effects (Meggio et al., 1995; Omura et al., 1995). The structures of the complexes that we here report should provide the basis for the rational development of novel, more specific PI3K inhibitors.

Results and Discussion

All of the inhibitors we investigated are competitive inhibitors of ATP binding. Because the porcine and human enzymes have 95.3% overall sequence identity and complete identity in the ATP binding pocket, there are no apparent structural differences between these two species in this region. We measured affinities of PI3Kγ for the reversible inhibitors quercetin, myricetin, LY294002, and staurosporine. The K_ds are generally comparable to the IC_{50}s that have been reported previously for other PI3K isozymes (Figure 1). As with the
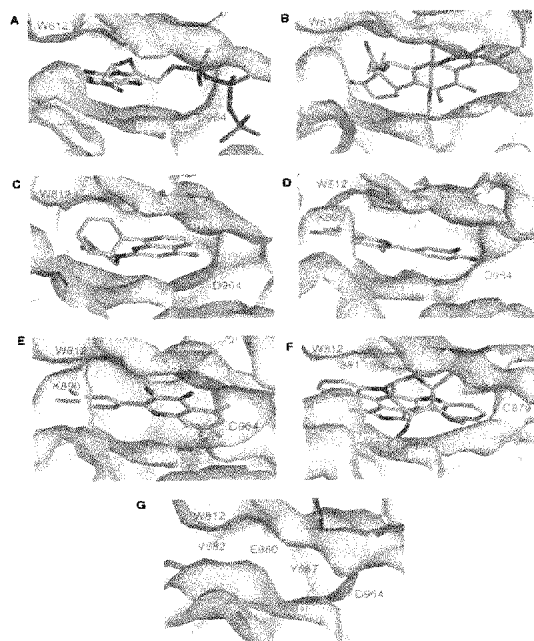
Figure 3. Interactions between Inhibitors and the PI3K Active Site

Each of the complexes was superimposed on the ATP/enzyme complex using the α-carbons of the N-terminal lobe. The molecular surfaces of the enzymes are shown. The complexes represented are PI3K with (A) ATP, (B) wortmannin , (C) LY294002, (D) quercetin, (E) myricetin, and (F) staurosporine. (G) The free human PI3K active site is illustrated.

Figure 4. A Comparison of Binding Modes in the PI3Kγ Active Site

The inhibitor/enzyme complexes were superimposed on the ATP/enzyme complex using the α-carbons of the N-terminal lobe of the catalytic domain. On the left, the inhibitors are shown superimposed on ATP (green). The region of the $2mF_o$-DF_c electron density maps for each of the compounds is illustrated on the right.

protein kinases, the ATP binding site of PI3K is located in a cleft between the N- and the C-terminal lobes of the catalytic domain (Figure 2). The structures show that each of the inhibitors binds in this site, with one ring system partially overlapping and coplanar with the space occupied by the adenine moiety of ATP (Figures 3, 4, and 5). All of the inhibitors have a hydrogen bond acceptor in a position equivalent to N1 of ATP. This is a feature that seems to be conserved in all kinase-inhibitor complexes (Lawrie et al., 1997). This interaction in PI3K involves the backbone of Val-882 and the 17-keto oxygen of wortmannin, the morpholino oxygen of LY294002, the ketone oxygen of quercetin, the hydroxyl oxygens of the phenyl moiety of myricetin, and the lactam nitrogen of staurosporine. None of the inhibitors extend into the space analogous to the volume occupied by the β and γ phosphates of ATP in the PI3K/ATP complex. All of the structures extend into a region that has been designated as hydrophobic region I in the protein kinases. This region that is opposite to the ribose binding region is delimited by Tyr-867 and Ile-879 in PI3Kγ (Figures 4 and 5). All of the inhibitors make more extensive interactions with this site than the ATP does.

Wortmannin Binding

Wortmannin binds in the ATP binding site so that one face of wortmannin packs against the N-terminal lobe (residues 831, 879, 881, and 882) and the other face
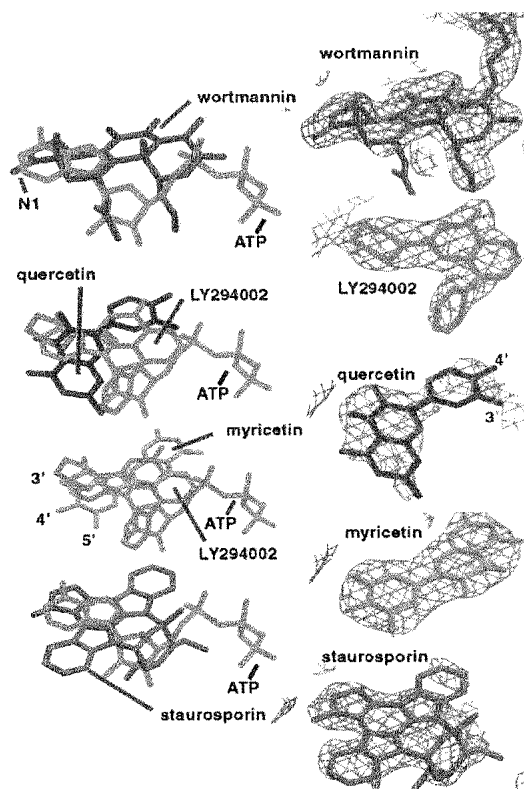
packs against the C-terminal lobe (residues 950, 953, 961, 963, and 964). One edge of wortmannin is adjacent to residues 867 and 841, while the opposite edge is exposed to solvent along most of its length (Figures 3B and 5B). The primary amine of active site Lys-833 attacks wortmannin at the furan ring (Wymann et al., 1996). The resulting covalent complex, which irreversibly inhibits the enzyme, is clearly seen in the electron density map (Figure 4).

In comparison with LY294002, quercetin, myricetin, and staurosporine, wortmannin causes a fairly large conformational rearrangement in the active site (Figure 6A). Binding of wortmannin and covalent modification of Lys-833 causes a movement of residues 832–838 and 871–876 away from the ATP binding pocket. This movement is associated with the rotation of the side chains of Phe-832 and His-834 that pack against Leu-742 and Thr-746 of helix kα1. This results in a coordinated movement of helix kα1 away from the ATP binding pocket. In addition, residues 748–750 at the C-terminal end of kα1 lose their α-helical conformation, and Glu-755 in the loop C-terminal to kα1 becomes oriented toward Lys-808 (Figure 6A).
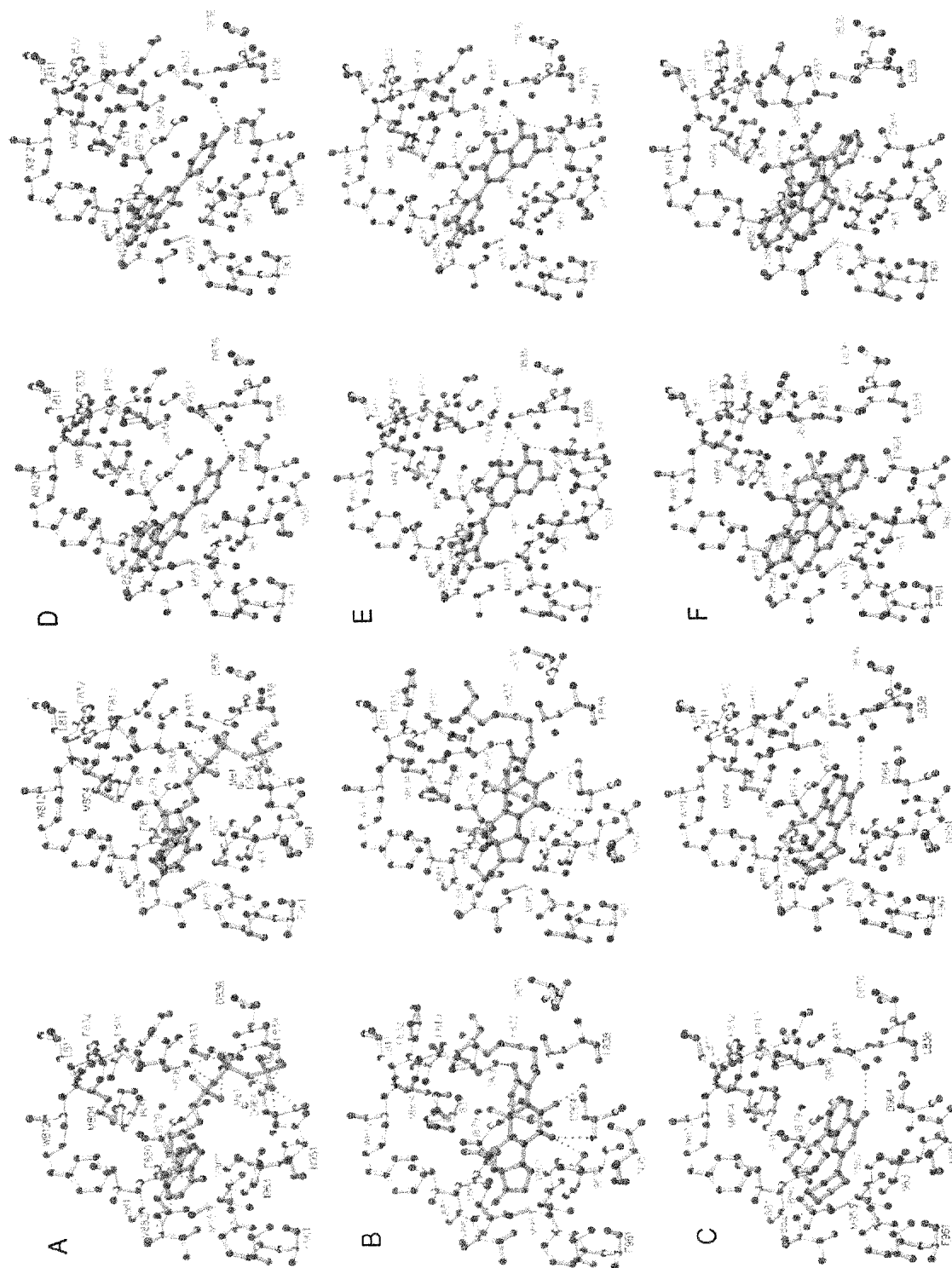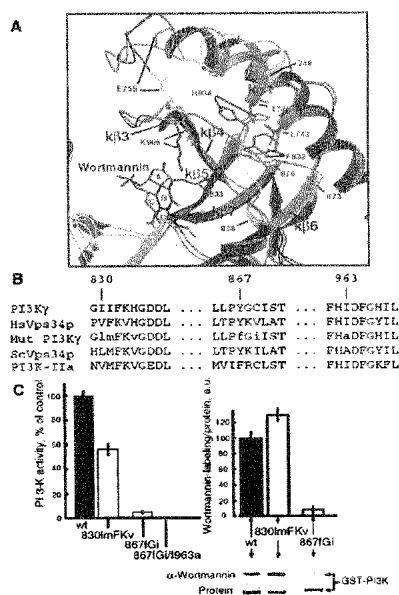
Figure 5. Stereoplots of the Active Sites of the PI3K Inhibitor Complexes

Hydrogen bonds are shown as red dotted lines. (A) ATP, (B) Wortmannin, (C) LY294002, (D) Quercetin, (E) Myricetin, (F) Staurosporine.

Figure 6. Wortmannin Inhibition of PI 3-Kinase

(A) Conformational changes upon wortmannin binding. The ATP/enzyme complex (green) and wortmanin/enzyme (red) complexes were superimposed using α-carbons of the N-terminal lobe. The three regions of the wortmannin/enzyme complex that show the greatest conformational changes relative to the ATP/enzyme complex are colored yellow. The "activation loop" (964–983) that is only partially ordered in both complexes is shown in purple.

(B) Sequences of two ATP binding site regions with sequence variation characteristic of enzymes that show reduced wortmannin sensitivity. The human Vps34p (HsVps34p) and PI3Kγ (PI3Kγ) have nanomolar IC₅₀s for wortmannin, whereas yeast Vps34p (ScVps34p) and the type IIα PI3K (PI3K-IIα) have much reduced sensitivities. The sequences of mutants that were tested for wortmannin binding and lipid kinase activity are indicated on the line labeled "Mut PI3Kγ." Lowercase letters indicate positions that were mutated relative to PI3Kγ. Three mutants were constructed: 830ImFKv834, 867fGi869, and 867fGi869/I963a.

(C) Lipid kinase activity and wortmannin reactivity of GST-fusion proteins of PI3Kγ and mutants. For the activity measurements, the production of PtdIns 3-P was monitored in vitro in the presence of 100 μM ATP. Results are displayed as a percentage of the wild-type control and represent means of five experiments (±SE) using three independent protein preparations (see Experimental Procedures). For wortmannin reactivity, immobilized PI3Kγ was incubated with 100 nM wortmannin. After removal of unreacted inhibitor, samples were denatured, applied to SDS-PAGE, blotted, and visualized with anti-wortmannin antibody. The bar graph represents the mean of three experiments (±SE). A representative immunoblot is also shown.

There is a close shape complementarity between the PI3K active site and wortmannin. Both of the methyl groups of wortmannin fit into small, hydrophobic pockets in the N-terminal lobe. The C13 methyl fits into a pocket made by residues 831, 879, 880, and 881, while the C10 methyl fits into a pocket made by residues 804, 810, and 831. These hydrophobic pockets are not occupied in the ATP structure. Although the binding of wortmannin to PI3K appears to be mainly through hydrophobic interactions, wortmannin forms five possi-

ble hydrogen bonds with PI3K (Figure 5B). These hydrogen bonds involve the oxygens attached to the steroid ring system: the ketone oxygen of the B ring interacts with the backbone of Asp-964 and with the hydroxyl of Tyr-867; the ketone oxygen of the D ring interacts with the backbone of Val-882; the ketone oxygen of the A ring interacts with the hydroxyl of Ser-806; and the hydroxyl of the B ring interacts with Asp-964 (this hydroxyl is the ether oxygen of the furan ring in the unreacted wortmannin).

Wortmannin binds more deeply in the ATP binding pocket than ATP. However, it has several interactions in common with the ATP/enzyme complex: the D ring ketone oxygen of wortmannin is located in a similar place to N1 of ATP; the acetytoxy group is in the volume corresponding to that occupied by the ribose of ATP (pointing out into solution); and the lactone oxygen of the A ring is in a similar position to the bridging oxygen of the α phosphate of ATP. Although no portion of wortmannin extends into the region of the active site occupied by the phosphates of ATP, PtdIns(4,5)-P₂ binding effectively competes with wortmannin binding (Wymann et al., 1996). One explanation for this may be that after PtdIns(4,5)-P₂ binding occurs, the enzyme undergoes a conformational change to close tightly on the bound PtdIns(4,5)-P₂. This conformational change that prevents water from competing for the phosphoryl transfer would then prevent an ATP analog from binding to the enzyme in the presence of PtdIns(4,5)-P₂. Despite extensive efforts, we have not been able to crystallise PI3Kγ in the presence of phospholipid substrate analogs, so this hypothesis cannot yet be structurally verified.

Numerous studies have been performed with wortmannin analogs to try to elucidate the mechanism of wortmannin binding. The analog 17β-hydroxywortmannin had higher affinity for PI3K than wortmannin itself (Norman et al., 1996). The replacement of the D ring ketone group with a hydroxyl would allow the formation of an additional hydrogen bond with the backbone nitrogen of residue Val-882. Introduction of the corticoid side chain at C17 prevents inhibition (Wiesinger et al., 1973) and would sterically be hindered by residues 881 and 882. Other modifications of the D ring of wortmannin, such as the addition of a bromo, hydroxyl, or acetyl group at position 16, dramatically decreased the affinity for PI3K. C16 is in contact with the side chain of Phe-961 and Val-882, and this result suggests that the decreased affinity is due to steric clashes with these residues.

The acetoxy group of the bound wortmannin is not visible in the electron density map. However, modeling the acetoxy group shows that this group would be located in an extensive hydrophobic environment. The C11 to which the acetoxy group is attached makes only one limited van der Waals contact with the enzyme via the side chain of Met-804. This is consistent with the observation that the desacetoxywortmannin binds only slightly more weakly than wortmannin (16.7 nM versus 4.2 nM) (Powis et al., 1994). However, substituting more lipophilic groups such as a butyryl group for the acetoxy group increases affinity of the compound for PI3K (Creemer et al., 1996). This is probably the result of the larger group interacting with the conserved hydrophobic pocket created by the side chains of Met-804, Trp-812, Ile-881, and Met-953.
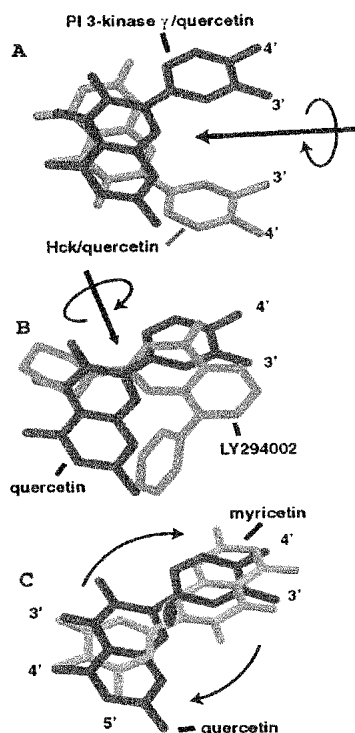
Figure 7. Illustration of the Relationships of the Orientation of the Chromone Moieties to Each Other in the Various Complexes Observed

For each panel, the structures containing the compounds were superimposed on each other using the C_α coordinates of the N-lobe of the catalytic domain. The arrow indicates the location of the approximate dyad axis relating one structure's binding mode to another.

(A) Quercetin binding in the protein kinase Hck as compared with PI3Kγ.

(B) Quercetin binding in PI3Kγ as compared to LY294002 binding to PI3Kγ.

(C) Myricetin binding to PI3Kγ as compared with quercetin binding to PI3Kγ.

Wortmannin covalently modifies PI3K by nucleophilic attack of NZ of Lys-833. This irreversible modification is an important determinant of the low nanomolar IC_{50} of wortmannin for PI3K. The furan ring of wortmannin is essential for its biological activity (Baggiolini et al., 1987), and when it is replaced by a pyran ring, the resulting inhibitor has only moderate affinity (Norman et al., 1996). Addition of a methyl group at C21 results in a compound that does not inhibit PI3K (Norman et al., 1996). This compound cannot covalently modify the enzyme but may also be prevented from binding in the active site by steric hindrance with the side chain of Lys-833 or Asp-964.

Isozyme Variation in Wortmannin Sensitivity

The class III PI3K Vps34p shows a striking species-dependent sensitivity to inhibition by wortmannin. In contrast to human Vps34p, yeast Vps34p is rather insen-

sitive to wortmannin (IC_{50} 3μM) and to LY294002 (IC_{50} 50 μM) (Stack and Emr, 1994). Based on the structure of PI3Kγ, homology models of the yeast and human Vps34p were constructed. This was also done for the class II PI3K PI3K-IIα, which shows reduced sensitivity to wortmannin (Virbasius et al., 1996; Domin and Waterfield, 1997). With the objective of designing a class IB enzyme that is less sensitive to wortmannin, a limited set of mutants were constructed that incorporated elements derived from the wortmannin-insensitive PI3Ks. There are two regions where residues in yeast Vps34p differ from the human Vps34p and are predicted to be in contact with ATP and wortmannin; the first is adjacent to the lysine corresponding to Lys-833 in PI3Kγ, where Ile-831 is replaced by a methionine in yeast Vps34p (Figure 6B). If the structure were to vary only in side chain rotamers, this replacement would presumably eliminate the space for wortmannin but not for ATP (because of the C10-methyl of wortmannin). When this region of contact was replaced in PI3Kγ by 830lmFKv (lower and upper case letters referring to mutated and unchanged residues, respectively), the enzyme retained about 55% of its activity. This result indicated that ATP could still be accommodated in the binding pocket. However, wortmannin binding, as assayed by the covalent reaction of the inhibitor with PI3Kγ, increased to 130% compared to binding of the wild-type protein. This suggests that there is enough flexibility in the enzyme or mode of binding to accommodate wortmannin. The second region we examined is 867YGC. Here, wortmannin-insensitive PI3Ks display YKI (yeast Vps34p) and FRC (PI3K-IIα). The isoleucine at the position equivalent to 869 in PI3Kγ might be expected to cause Tyr-867 to adopt a different rotamer and eliminate the interaction of the hydroxyl of Tyr-867 with the ketone group of the B ring of wortmannin. The replacement of the tyrosine with a phenylalanine would also eliminate this interaction. This agrees with the fact that the 867fGi mutation eliminates wortmannin binding. However, lipid kinase activity was also reduced to less than 10% of the wild-type enzyme, and this result indicated that Tyr-867 cannot be replaced without further compensations. An I963A mutation was introduced to create space for an alternative rotamer for Phe-867, but Ile-963 seems to be necessary for the integrity of the catalytic site because this mutant completely abolished activity.

This limited set of mutants provides some indication as to the extent to which the enzyme structure is able to adapt to mutations. The results suggest that the region around Tyr-867 might be relatively rigid. In contrast, residues in the region 830–835 might have more flexibility that could be exploited in the design of novel inhibitors occupying even more space than wortmannin.

LY294002 Binding

LY294002 is a synthetic inhibitor of PI3Ks. An IC_{50} for this inhibitor of 1.4 μM has been measured for a class IA PI3K (Vlahos et al., 1994). For PI3Kγ, we have measured a K_d of 0.21 μM. The structure of the complex of LY294002 with PI3Kγ provides a framework for understanding the structure/activity relationships that have been reported for LY294002 and related compounds (Vlahos et al., 1994). The morpholino ring of LY294002

Table 1. Data Collection, Structure Determination, and Refinement Statistics

Data Set[g]	Resolution (Å)	Observations/ Unique Reflections	Completness (Last Shell) (%)	R_{merge}[h]	$<I/\sigma>$ (Last Shell)	Number of Reflections Used for R_{free}
Wortmannin[a]	2.0	227,525/68,705	97.4 (94.2)	8.3	16.01 (1.1)	2686
LY294002[b]	2.4	110,067/33,528	85.4 (39.2)	7.0	20.49 (1.3)	1630
Quercetin[c]	2.5	116,715/34,614	97.5 (83.1)	5.9	22.55 (2.14)	1706
Myricetin[d]	2.7	95,921/27,535	99.3 (99.4)	4.8	17.14 (7.1)	1409
Staurosporine[e]	2.4	103,376/32,910	87.7 (57.7)	8.7	18.94 (3.28)	1935
Human native[f]	2.0	176,129/58,245	92.8 (72.9)	7.9	16.50 (2.32)	2284

Refinement Statistics

Data Set	Resolution (Å)	Protein Atoms	Waters	R_{cryst}[i]	R_{free}[i] (% Data Used)	Rmsd from Ideality[j] Bonds	Angles	Dihedrals
Wortmannin	25.0–2.0	7,046	164	0.25	0.29 (3.9)	0.0074 Å	1.1°	21°
LY294002	25.0–2.4	6,890	136	0.27	0.30 (4.9)	0.0077 Å	1.1°	22°
Quercetin	25.0–2.5	6,916	0	0.26	0.33 (4.9)	0.021 Å	1.9°	24°
Myricetin	25.0–2.7	6,839	0	0.27	0.30 (6.2)	0.0053 Å	1.0°	21°
Staurosporine	25.0–2.4	6,802	40	0.23	0.29 (5.9)	0.014 Å	1.4°	23°
Human native	25.0–2.0	6,816	148	0.22	0.29 (3.9)	0.016 Å	1.6°	23°

[a] The wortmannin crystal was soaked in 1 mM wortmannin for 50 min.

[b] The LY294002 crystal was soaked in 1 mM LY294002 for 200 min.

[c] The quercetin crystal had 1.5 μl of cryoprotectant followed by 1 μl of 1 mM quercetin added to the drop in which the crystal had grown. Total exposure time to quercetin was 110 min.

[d] The crystal was soaked for 2 hr in 1 mM myricetin.

[e] The crystal was soaked in 1 mM staurosporine for 150 min.

[f] The native human crystal was soaked in 1 mM demethoxyviridin for 180 min. This data set did not have density corresponding to demethoxyviridin. This absence of bound compound is due to the reactivity of demethoxyviridin with the Tris buffer used for crystal growth.

[g] All data sets were collected at ESRF beamline ID14-2 except for myricetin, which was collected at ID14-1.

[h] $R_{merge} = \Sigma_{hkl}\Sigma_i|I_{i(hkl)} - <I_{(hkl)}>|/\Sigma_{hkl}\Sigma_i I_{i(hkl)}$

[i] R_{cryst} and $R_{free} = \Sigma |F_{obs} - F_{calc}|/\Sigma F_{obs}$; R_{free} is calculated with the percentage of the data shown in parentheses.

[j] Rmsd for bond angles and lengths in regard to Engh and Huber parameters.

partially overlaps the volume occupied by the adenine in the ATP/enzyme complex (Figures 3C, 4, and 5C). There is a hydrogen bond between the morpholino oxygen and the backbone amide of residue 882, and this bond mimics the interaction that N1 of ATP makes with the enzyme. Loss of this interaction is presumably the reason that analogs lacking a hydrogen bond acceptor at this position are poor inhibitors. The chromone (benzopyran-4-one) scaffold of LY294002 is approximately coplanar with the adenine ring of ATP. There is a putative hydrogen bond between NZ of Lys-833 and the ketone moiety. Removal of the phenyl ring decreases inhibition approximately 3-fold. Occupying a similar space as the ribose of ATP, the 8-phenyl ring packs against Met-804 and Trp-812 on one side and Met-953 on the other. LY294002 does not extend into the phosphate binding region. The presence of the putative hydrogen bond between the side chain of Lys-833 and the ketone means that there is less free space on the ketone side of the chromone ring system. This explains why a 5-6 fused phenyl derivative was a poorer inhibitor than a 7-8 fused phenyl derivative.

The K_d of PI3Kγ for LY294002 is 0.21 μM, similar to the affinity of the enzyme for the broad-spectrum protein kinase inhibitor quercetin (K_d = 0.28 μM, Figure 1). However, LY294002 is a specific inhibitor for PI3Ks, and at a concentration of 50 μM, LY294002 has no inhibitory effect on a range of protein kinases, including the c-AMP-dependent protein kinase and c-Src (Vlahos et al., 1994). Examination of the structures of these enzymes suggests that one determinant of this specificity may be the bulky 8-phenyl group of LY294002. The phenyl group occupies a space corresponding to the ribose of ATP (Figures 3C, 4, and 5C). The active site of PI3K is more open at this position than in the protein kinases, and PI3K makes only limited contact with the ribose moiety (Figures 3A and 5A). LY294002 probably cannot be well accommodated in the protein kinases that make more extensive interactions with the ribose and that, consequently, have less space in this region.

Quercetin Binding

The plant-derived bioflavonoid quercetin [2-(3,4-dihydroxyphenyl)-3,5,7-trihydroxy-4H-1-benzopyran-4-one] is a broad-spectrum protein kinase inhibitor. In the PI3K/quercetin complex, the electron density for quercetin has a boomerang shape with a larger and a smaller lobe. The model for the enzyme/quercetin structure was constructed so that the chromone moiety fills the larger lobe of the boomerang (Figure 4). This density unambiguously defines the position and plane of the quercetin. However, the dihydroxyphenyl moiety is incompletely defined. This may indicate that the compound binds in more than one orientation.

Quercetin has previously been crystallized with the tyrosine kinase Hck (Sicheri et al., 1997) (PDB entry 2HCK). Relative to the Hck/quercetin complex, the PI3K complex has a shift in the quercetin so that the chromone appears to make three hydrogen bonds with the backbone of residues 880–882 in the linker region (Figure 5D). Two of these hydrogen bonds are formed with the chromone 3- and 5-hydroxyls. Consistent with the PI3Kγ structure is the observation that substitutions at the 3 position decrease the IC_{50} (Matter et al., 1992).

Additionally, the ketone moiety interacts with the amide of Val-882 in a manner analogous to the N1 of the ATP adenine. In the Hck/quercetin complex, the analogous interaction involves the 5-hydroxyl of the chromone, while the ketone oxygen forms no apparent hydrogen bond. This means that the quercetin in the Hck complex is flipped by 180° relative to the quercetin in the PI3K complex (Figure 7A).

Although quercetin was the lead compound on which a variety of derivatives, including LY294002, were designed (Vlahos et al., 1994), it appears that the interactions of these two compounds with PI3K are quite different. The chromone moiety of quercetin occupies the space filled by the morpholino ring of LY294002 (Figures 3 and 4). The 3',4'-dihydroxyphenyl moiety at the 2 position of quercetin makes a putative hydrogen bond with NZ of Lys-833, and the most potent analogs of quercetin have this dihydroxy substitution of the phenyl group (Gamet-Payrastre et al., 1999). The hydrogen bond between the 3'-OH of quercetin and the side chain of Lys-833 mimics the interaction made by the ketone moiety of LY294002. This means that the chromone moiety of LY294002 is flipped 180° with respect to mode of binding in the quercetin/PI3K complex (Figure 7B). The flip of the LY294002 orientation relative to quercetin is possibly a consequence of the nonplanar morpholino group. If the LY294002 were to bind in a manner strictly analogous to the quercetin, then the morpholino ring would sterically clash with the backbone of Asp-964.

Myricetin Binding

Myricetin (3,5,7-trihydroxy-2-(3,4,5-trihydroxyphenyl)-4H-1-benzopyran-4-one), another naturally occurring flavonoid, differs from quercetin only by the addition of a hydroxyl at the 5'-OH of the phenyl moiety. Using class IA PI3K, studies of this compound indicated that it is a more tightly binding inhibitor than quercetin (Gamet-Payrastre et al., 1999). For PI3Kγ, our measurements showed that myricetin has a K_d of 0.17 μM, which is slightly lower than that of quercetin. The electron density for myricetin is best fit by a model having the compound flipped end-for-end relative to the binding we observed for quercetin (Figures 3E, 4, 5E, and 7C). In this orientation, the 3' and 4' hydroxyls of the phenyl moiety make interactions with the backbone of Val 882 that are analogous to interactions made by the chromone moiety of quercetin and the N1 of adenine in the ATP complex (Figures 4 and 5E). The chromone moiety of myricetin interacts with the side chains of Asp-964, Tyr-967, and Lys-833. The interaction of the hydroxyl of the chromone moiety with Lys-833 (Figure 5E) is analogous to the interaction of this residue with the 3' OH of quercetin (Figure 5D). Although LY294002, myricetin, and quercetin bind so that the chromone moieties are in approximately the same plane, the variety of orientations that we observe within this plane is probably largely the consequence of the approximately symmetric arrangement of hydrogen bond donors and acceptors in these compounds. The somewhat greater number of possible hydrogen bonds between the protein and myricetin as compared with quercetin may account for the tighter binding observed for myricetin. It may be possible to design analogs that would be capable of simultaneously forming the interactions exhibited by quercetin and myricetin.

Staurosporine Binding

The position of staurosporine binding to PI3K (Figures 3F, 4, and 5F) largely resembles the position of staurosporine binding to the protein kinases (Lawrie et al., 1997; Prade et al., 1997; Lamers et al., 1999; Zhu et al., 1999). The K_d for staurosporine binding to human PI3Kγ is 0.29 μM (Figure 1). The majority of the interactions are hydrophobic, although there are some apparent hydrogen bonds. The staurosporine lactam nitrogen occupies a space analogous to the N6 of ATP, and the lactam oxygen mimics the interaction of ATP N1 with the backbone of Val-882 (Figure 4). There is no electron density visible for the methylamino group of the staurosporine. However, the density corresponding to the sugar moiety of the staurosporine is better fit by a chair conformation than a boat conformation (Figure 4). Studies of this compound in solution show that both conformers exist, but that there is a preference for the boat conformer (Davis et al., 1991). The crystal structures of the C-terminal domain of Src kinase and cyclin-dependent protein kinase 2 (CDK2) show the compound bound in the boat conformation (Lawrie et al., 1997; Lamers et al., 1999).

Staurosporine has a range of affinities for different kinases. It has nanomolar potency against many protein kinases such as c-AMP-dependent protein kinase A (cAPK) and CDK2, but it has micromolar potency against casein kinases 1 and 2 (CK1 and CK2), mitogen-activated protein kinase (MAPK), and CSK (Lamers et al., 1999). Because the area of contact between staurosporine and the enzyme is roughly the same for both groups of enzymes, this difference has been attributed to the presence of an additional hydrogen bond to the methylamino nitrogen of staurosporine in the high-affinity binding proteins (Lamers et al., 1999). This putative high-affinity interaction involves Glu-127 in cAPK. The equivalent residue in the low-affinity staurosporine binding kinases is a serine (e.g., Ser-273 in CSK). In the class I PI3Ks, this residue is Thr-886. As with the low-affinity staurosporine binding protein kinases, this residue does not interact with the bound inhibitor. The chair conformation of the inhibitor allows for a putative hydrogen bond between the methoxy moiety of staurosporine and the side chain of Asp-964.

Conclusion

The structures described here reveal a set of interactions that are common to both ATP and the inhibitors. Moreover, they show a variety of unique interactions exploited by the inhibitors. Both sets of observations will be important for design of more specific PI3K inhibitors. The results of the mutagenesis and the conformational changes evident upon binding wortmannin suggest that there is flexibility in the structure of the catalytic domain that might also be exploited in inhibitor design. This will undoubtedly require more extensive mutagenesis, inhibitor design, and structural analysis.

Experimental Procedures

Protein Expression and Purification for Crystallographic Studies
A construct encoding residues 144 to the C terminus (1102) of the catalytic subunit of porcine PI3Kγ was expressed and purified as described previously (Walker et al., 1999). The same N-terminal deletion variant encoding human PI3Kγ, but with a directly fused

C-terminal His$_6$-tag, was cloned into pVL1393 (Invitrogen). Each construct was transfected into baculovirus and expressed in Sf9 cells. The cells were infected at 27°C for up to 72 hr, harvested, washed in PBS containing 100 μM AEBSF (Melford Laboratories), snap frozen in liquid nitrogen, and stored at −80°C. The human PI3Kγ was purified in three chromatographic steps: immobilized metal affinity chromatography on a Talon resin (Clonetech), cation exchange, and gel filtration. Frozen cells from 2.7 L of Sf9 cell culture were resuspended in sonication buffer (50 mM KH$_2$PO$_4$ [pH 8], 10 mM Tris [pH 8], 100 mM NaCl, 1 mM MgCl$_2$) and lysed by sonication in the presence of protease inhibitors (complete EDTA-free tablets, Boehringer Mannheim). The lysate was centrifuged at 100,000 g for 1 hr, and the supernatant was incubated with 2.5 ml of Talon resin for 1 hr. The resin was then washed four times with 50 ml of solution 1 (50 mM KH$_2$PO$_4$ [pH 8], 20 mM Tris [pH 8], 0.1 M NaCl, 1% betaine, 0.05% Tween 20), five times with 50 ml of solution 2 (50 mM KH$_2$PO$_4$ [pH 7.0], 20 mM Tris [pH 7.5], 0.1 M NaCl, 1% betaine, 0.05% Tween 20), and four times with 50 ml of solution 3 (20 mM Tris [pH 7.5], 13.4 mM imidazole, 0.1 M NaCl, 1% betaine, 1% ethylene glycol). Protein was eluted with elution buffer (20 mM KH$_2$PO$_4$ [pH 5.6], 0.1 M EDTA, 1% betaine, 1% ethylene glycol, and 0.02% CHAPS). The Talon eluent was then loaded on a Poros 20HS cation exchange column and eluted with a 0–1 M NaCl gradient in 20 mM KH$_2$PO$_4$ [pH 5.6], 1 mM DTT. The protein was further purified by gel filtration on a Pharmacia 16/60 Superdex 200 column equilibrated in 20 mM Tris [pH 7.2], 50 mM (NH$_4$)$_2$SO$_4$, 1% betaine, 1% ethylene glycol, 0.02% CHAPS, and 5 mM DTT. The protein was concentrated to 4 mg/ml (BioRad protein assay) and frozen in liquid nitrogen.

Constructs for Lipid Kinase Assays and Wortmannin Binding

PI3K mutant expression plasmids were constructed with a CMV-driven GST-PI3Kγ fusion-protein vector (pSTC-tkGST<p110γ E/A>) (Stoyanova et al., 1997) with two artificially introduced silent restriction sites, EagI and AvrII (Bondeva et al., 1998). The mutations indicated in Figure 6B were introduced by overlap extension (Ho et al., 1989), and PCR fragments were cloned into the EagI/AvrII sites of pSTC-tkGST<p110γ E/A>. The amplified regions were verified by DNA sequencing (Microsynth, Balgach, Switzerland). GST-PI3Kγ was expressed by transient transfection of HEK293 cells as in Wymann et al., 1996 and Stoyanova et al., 1997. Briefly, cells were lysed 48 hr after calcium phosphate transfection with lysis buffer (20 mM Tris·HCl [pH 8.0], 138 mM NaCl, 2.7 mM KCl, 5% glycerol, 1 mM sodium orthovandate, 20 μM leupeptin, 18 μM pepstatin, 1% NP-40, 5 mM EDTA, and 20 mM NaF). Cleared supernatants were incubated with glutathione-Sepharose (Pharmacia) to immobilize PI3Kγ. For activity measurements, the protein was released from washed beads by incubation with lysis buffer (without supplements) containing 5 mM reduced glutathione. PI3K was stored in 50% polyethyleneglycol, 10 mM Tris·HCl pH 7.5, 1 mM EDTA, 5 mM benzamidine, and 1 mM dithiothreitol at −20°C until use. PI3K activity was assayed with PtdIns (PtdIns/PtdSer mixture) and [^{32}P]γATP as substrates. PtdIns 3-P was separated on thin-layer chromatography and quantified on a Personal-FX imager (BioRad) (Wymann et al., 1996). For wortmannin binding assays, immobilized PI3K was incubated with 100 nM wortmannin in phosphate-buffered saline (PBS) for 15 min on ice, washed twice with PBS supplemented with 0.01% Triton X-100, and applied to denaturing SDS-PAGE and anti-wortmannin immunoblotting essentially as described in (Wymann et al., 1996). The protein on PVDF membranes was quantified by colloidal gold staining (BioRad). Anti-wortmannin and total protein signals were quantified on a GS-700 Imaging Densitometer (BioRad).

Crystallization and Inhibitor Soaks

PI3K crystals were grown at 17°C by the hanging-drop vapor-diffusion method by mixing 1 μl of PI3K with 1 μl of reservoir solution. The reservoir for the porcine PI3K consisted of 100 mM Tris·HCl [pH 7.2], 200 mM Li$_2$SO$_4$, and 14%–15% PEG 4000. Crystals were obtained by hair seeding. The reservoir for the human PI3K crystals consisted of 0.1 M Tris [pH 7.2], 250 mM (NH$_4$)$_2$SO$_4$, and 19% PEG 4000. Crystals were initially obtained by hair seeding from porcine PI3K crystals. The crystals reached their maximum size (0.2 mm × 0.1 mm × 0.1 mm) in about 10 days.

LY294002, staurosporine (Alexis Pharmaceuticals), quercetin (Aldrich), and myricetin (Fluka) stocks were prepared in DMSO, and a wortmannin (Alexis Pharmaceuticals) stock was prepared in methanol. Inhibitor stocks were diluted in cryoprotectant [200 mM Li$_2$SO$_4$, 100 mM Tris·HCl [pH 7.2], 20% PEG 4000, and 12% glycerol; or 100 mM Tris [pH 7.2], 250 mM (NH$_4$)$_2$SO$_4$, 25% PEG 4000, and 15% glycerol for the porcine and human crystals, respectively] to a final concentration of 1 mM. Inhibitor in cryoprotectant was slowly added to the drop in which the crystals were grown. The crystal was then transferred to the 1 mM inhibitor solution in cryoprotectant for the time specified in Table 1. Crystals were then transferred to fresh inhibitor/cryoprotectant for 30 s and frozen in a stream of N$_2$ at 100 K.

Data Collection and Structure Determination

Data sets were collected at ESRF beamlines ID14-1 (Mar CCD), ID-14-2 (Mar CCD), and ID14-4 (ADSC CCD). The images were processed with MOSFLM (Leslie, 1992) and scaled with Scala (CCP4, 1994). For the porcine PI3K, initial phases for the inhibitor/enzyme complexes were obtained from the isomorphous enzyme/ATP complex. Because of a 4% shrinkage of the a and c axes, the human PI3K data sets were not isomorphous to the porcine PI3K data. Initial phases were obtained using molecular replacement with AMORE and the model of the porcine PI3Kγ. The initial model for each complex was first refined as six rigid bodies in CNS (representing the N-terminal linker, the Ras binding domain, the C2 domain, the helical domain, and the N- and C-terminal lobes of the catalytic domain). The models were then refined as rigid bodies representing each secondary-structural element. The initial models were finally refined as individual atoms. Manual rebuilding in O (Jones et al., 1991) was then alternated with CNS refinement (Brunger et al., 1998).

Fluorescence Assays for Determination of Binding Affinity

Binding was detected as a change in the intrinsic tryptophan fluorescence ($\lambda_{ex} = 280$ nm, $\lambda_{em} = 340$ nm) of the PI3K upon the addition of inhibitor. Solutions having 0.033 μM PI3K, 20 mM Tris [pH 7.2], 2 mM MgCl$_2$, 1 mM DTT, and 0.5% DMSO were prepared. The inhibitor was incubated with the protein for at least 15 min before the fluorescence intensity was measured. For each concentration of inhibitor, fluorescence data were acquired for 30 s and averaged. The fluorescence of a solution containing all of the components except inhibitor was subtracted from each measurement. For staurosporine, which has a slight fluorescence at the same wavelength as tryptophan, the fluorescence of staurosporine in the same buffer without protein was also subtracted from each measurement. All measurements were carried out at 20°C. Data were fitted to a binding equation to obtain dissociation constants (using nonlinear least-squares fitting in Kaleidograph).

References

Agullo, G., Garnet-Payrastre, L., Manenti, S., Viala, C., Rémésy, C., Chap, H., and Payrastre, B. (1997). Relationship between flavonoid structure and inhibition of phosphatidylinositol 3-kinase: a comparison with tyrosine kinase and protein kinase C inhibition. Biochem. Pharmacol. 53, 1649–1657.

Arcaro, A., and Wymann, M.P. (1993). Wortmannin is a potent phosphatidylinositol 3-kinase inhibitor: the role of phosphatidylinositol

3,4,5-trisphosphate in neutrophil responses. Biochem. J. *296*, 297–301.

Baggiolini, M., Dewald, B., Schnyder, J., Ruch, W., Cooper, P.H., and Payne, T.G. (1987). Inhibition of the phagocytosis-induced respiratory burst by the fungal metabolite wortmannin and some analogs. Exp. Cell Res. *169*, 408–418.

Bondeva, T., Pirola, L., Bulgarelli-Leva, G., Rubio, I., Wetzker, R., and Wymann, M.P. (1998). Bifurcation of lipid and protein kinase signals of PI3K gamma to the protein kinases PKB and MAPK. Science *282*, 293–296.

Brian, P.W., Curtis, P.J., Hemming, H.G., and Norris, G.L.F. (1957). Wortmannin, an antibiotic produced by *Penicillium wortmanni*. Trans. Br. Mycol. *40*, 365–368.

Brünger, A.T., Adams, P.D., Clore, G.M., DeLano, W.L., Gros, P. GrosseKunstleve, R.W., Jiang, J.S., Kuszewski, J., Nilges, M., Pannu, N.S., et al. (1998). Crystallography & NMR system: a new software suite for macromolecular structure determination. Acta Crystallogr. D *54*, 905–921.

Cantley, L.C., and Neel, B.G. (1999). New insights into tumor suppression: PTEN suppresses tumor formation by restraining the phosphoinositide 3-kinase AKT pathway. Proc. Natl. Acad. Sci. USA *96*, 4240–4245.

CCP4 (Collaborative Computing Project 4) (1994). The CCP4 suite: programs for protein crystallography. Acta Crystallogr. D *50*, 760–763.

Creemer, L.C., Kirst, H.A., Vlahos, C.J., and Schultz, R.M. (1996). Synthesis and *in vitro* evaluation of new wortmannin esters – potent inhibitors of phosphatidylinositol 3-kinase. J. Med. Chem. *39*, 5021–5024.

Davis, P.D., Hill, C.H., Thomas, W.A., and Whitcombe, I.W.A. (1991). The design of inhibitors of protein kinase C – the solution conformation of staurosporine. J. Chem. Soc., Chem. Commun. 3, 182–184.

Domin, J., and Waterfield, M.D. (1997). Using structure to define the function of phosphoinositide 3-kinase family members. FEBS Lett. *410*, 91–95.

Gamet-Payrastre, L., Manenti, S., Gratacap, M.-P., Tulliez, J., Chap, H., and Payrastre, B. (1999). Flavonoids and the inhibition of PKC and PI 3-kinase. Gen. Pharmacol. *32*, 279–286.

Garcia-Echeverria, C., Traxler, P., and Evans, D.B. (2000). ATP site-directed competitive and irreversible inhibitors of protein kinases. Med. Res. Rev. *20*, 28–57.

Gershtein, E.S., Shatskaya, V.A., Ermilova, V.D., and Kushlinsky, N.E. (1999). Phosphatidylinositol 3-kinase expression in human breast cancer. Clin. Chim. Acta *287*, 59–67.

Hirsch, E., Katanaev, V.L., Garlanda, C., Azzolino, O., Pirola, L., Silengo, L., Sozzani, S., Mantovani, A., Altruda, F., and Wymann, M.P. (2000). Central role for G protein-coupled phosphoinositide 3-kinase γ in inflammation. Science *287*, 1049–1053.

Ho, S.N., Hunt, H.D., Horton, R.M., Pullen, J.K., and Pease, L.R. (1989). Site-directed mutagenesis by overlap extension using the polymerase chain reaction. Gene *77*, 51–59.

Jones, T.A., Zou, J.-Y., Cowan, S.W., and Kjeldgaard, M. (1991). Improved methods for building protein models in electron density maps and the location of errors in these models. Acta Crystallogr. A *47*, 110–119.

Kraulis, P.J. (1991). MOLSCRIPT: a program to produce both detailed and schematic plots of protein structures. J. Appl. Crystallogr. *24*, 946–950.

Krugmann, S., Hawkins, P.T., Pryer, N., and Braselmann, S. (1999). Characterizing the interactions between the two subunits of the p101/p110γ phosphoinositide 3-kinase and their role in the activation of this enzyme by Gβγ. J. Biol. Chem. *274*, 17152–17158.

Lamers, M., Antson, A.A., Hubbard, R.E., Scott, R.K., and Williams, D.H. (1999). Structure of the protein tyrosine kinase domain of C-terminal Src kinase (CSK) in complex with staurosporine. J. Mol. Biol. *285*, 713–725.

Lawrie, A.M., Noble, M.E.M., Tunnah, P., Brown, N.R., Johnson, L.N., and Endicott, J.A. (1997). Protein kinase inhibition by staurosporine

revealed in details of the molecular interaction with CDK2. Nat. Struct. Biol. *4*, 796–801.

Leslie, A.G.W. (1992). Recent changes to the MOSFLM package for processing film and image plate data. Paper presented at: Joint CCP4 and ESF-EACMB Newsletter on Protein Crystallography (Daresbury Laboratory, Warrington, UK).

Li, Z., Jiang, H.P., Xie, W., Zhang, Z.C., Smrcka, A.V., and Wu, D.Q. (2000). Roles of PLC-β2 and -β3 and PI3Kγ in chemoattractant-mediated signal transduction. Science *287*, 1046–1049.

Maier, U., Babich, A., and Nürnberg, B. (1999). Roles of non-catalytic subunits in G βγ-induced activation of class I phosphoinositide 3-kinase isoforms β and γ. J. Biol. Chem. *274*, 29311–29317.

Matter, W.F., Brown, R.F., and Vlahos, C.J. (1992). The inhibition of phosphatidylinositol 3-kinase by quercetin and analogs. Biochem. Biophys. Res. Commun. *186*, 624–631.

Meggio, F., Donella-Deana, A., Ruzzene, M., Brunati, A.M., Cesaro, L., Guerra, B., Meyer, T., Mett, H., Fabbro, D., Furet, P., et al. (1995). Different susceptibility of protein kinases to staurosporine inhibition - kinetic studies and molecular bases for the resistance of protein kinase CK2. Eur. J. Biochem. *234*, 317–322.

Merritt, E.A., and Bacon, D.J. (1997). Raster3D: photorealistic molecular graphics. Methods Enzymol. *277*, 505–524.

Myers, M.P., Pass, I., Batty, I.H., Van der Kaay, J., Stolarov, J.P., Hemmings, B.A., Wigler, M.H., Downes, C.P., and Tonks, N.K. (1998). The lipid phosphatase activity of PTEN is critical for its tumour suppressor function. Proc. Natl. Acad. Sci. USA *95*, 13513–13518.

Norman, B.H., Shih, C., Toth, J.E., Ray, J.E., Dodge, J.A., Johnson, D.W., Rutherford, P.G., Schultz, R.M., Worzalla, J.F., and Vlahos, C.J. (1996). Studies on the mechanism of phosphatidylinositol 3-kinase inhibition by wortmannin and related analogs. J. Med. Chem. *39*, 1106–1111.

Omura, S., Sasaki, Y., Iwai, Y., and Takeshima, H. (1995). Staurosporine, a potentially important gift from a microorganism. J. Antibiot. *48*, 535–548.

Phillips, W.A., StClair, F., Munday, A.D., Thomas, R.J.S., and Mitchell, C.A. (1998). Increased levels of phosphatidylinositol 3-kinase activity in colorectal tumors. Cancer *83*, 41–47.

Powis, G., Bonjouklian, R., Berggren, M.M., Gallegos, A., Abraham, R., Ashendel, C., Zalkow, L., Matter, W.F., Dodge, J., Grindey, G., and Vlahos, C.J. (1994). Wortmannin, a potent and selective inhibitor of phosphatidylinositol- 3-kinase. Cancer Res. *54*, 2419–2423.

Prade, L., Engh, R.A., Girod, A., Kinzel, V., Huber, R., and Bossemeyer, D. (1997). Staurosporine-induced conformational changes of cAMP-dependent protein kinase catalytic subunit explain inhibitory potential. Structure *5*, 1627–1637.

Sasaki, T., Irie-Sasaki, J., Jones, R.G., Oliveira-dos-Santos, A.J., Stanford, W.L., Bolon, B., Wakeham, A., Itie, A., Bouchard, D., Kozieradzki, I., et al. (2000). Function of PI3K γ in thymocyte development, T cell activation, and neutrophil migration. Science *287*, 1040–1046.

Sicheri, F., Moarefi, I., and Kuriyan, J. (1997). Crystal structure of the Src family tyrosine kinase Hck. Nature *385*, 602–609.

Srivastava, A.K. (1985). Inhibition of phosphorylase-kinase, and tyrosine protein-kinase activities by quercetin. Biochem. Biophys. Res. Commun. *131*, 1–5.

Stack, J.H., and Emr, S.D. (1994). Vps34p required for yeast vacuolar protein sorting is a multiple specificity kinase that exhibits both protein-kinase and phosphatidylinositol-specific PI-3-kinase activities. J. Biol. Chem. *269*, 31552–31562.

Stephens, L.R., Eguinoa, A., Erdjument-Bromage, H., Lui, M., Cooke, F., Coadwell, J., Smrcka, A.S., Thelen, M., Cadwallader, K., Tempst, P., and Hawkins, P.T. (1997). The Gβγ sensitivity of a PI3K is dependent upon a tightly associated adaptor, p101. Cell *89*, 105–114.

Stoyanova, S., Bulgarelli-Leva, G., Kirsch, C., Hanck, T., Klinger, R., Wetzker, R., and Wymann, M.P. (1997). Lipid kinase and protein kinase activities of G-protein-coupled phosphoinositide 3-kinase γ: structure-activity analysis and interactions with wortmannin. Biochem. J. *324*, 489–495.

Toker, A., and Cantley, L.C. (1997). Signalling through the lipid products of phosphoinositide-3-OH kinase. Nature *387*, 673–676.